Entanglement via entangled-boundary-condition trajectories: long-time accuracy

A. J. S. Lara[1] and A. D. Ribeiro[1]

[1] *Departamento de Física, Universidade Federal do Paraná, 81531-990, Curitiba, PR, Brazil*

Entanglement is considered as a purely quantum effect. The present paper, however, joins many other works that pursue the idea of describing it using classical quantities. In particular, we are interested in the entanglement dynamics of a pure state, composed of two parts, initially prepared in a product of coherent states, and governed by a generic Hamiltonian. In this scenario, the linear entropy of the reduced state, our entanglement quantifier, was shown to be written, in the short-time regime, in terms of a *real* trajectory of the underlying classical dynamics. We extend this semiclassical result by demonstrating that it is possible to include *complex* trajectories in the calculation. This strategy contributes to improving the previous approximation, extending its accuracy for longer values of time. We also show, for a particular Hamiltonian, a first application of the achieved formula, attesting its efficiency.

PACS numbers: 03.67.Bg, 03.65.Sq, 03.65.Ud, 03.67.Mn

I. INTRODUCTION

The connection between quantum entanglement of a given physical system and features present in its classical description has attracted an enormous attention from researchers in the last twenty years. Such a fascination is intensified because entanglement, which is one of the main protagonists of the eminent quantum-information theory [1, 2], is usually considered as a purely quantum effect. Given the context, an interesting fundamental question naturally arises concerning the possible classical mechanisms associated with entanglement dynamics. Although there is a large number of approaches dealing with this issue in the literature, in the present paper we argue that it still deserves investigation.

Inspired by essential ideas of the quantum chaos theory [3, 4], in which, for instance, certain properties of the *quantum* energy spectrum crucially depend on the dynamical regime manifested by the *classical* description, many approaches were developed to establish a correlation between the behavior of the entanglement dynamics and the presence of chaos in the correspondent classical system. Following this program, some researchers have performed this characterization by directly comparing classical and quantum descriptions without defining a classical counterpart for entanglement [5–10], while others developed such classical figures of merit in order to quantitatively study the quantum-classical connection [11–18].

Alternatively, other authors have deviated from the focus on quantum chaos studies and followed the strategy of performing semiclassical approximations on a proper quantum description, in order to force the emergence of a classical connection with entanglement. This idea was implemented by means of time-dependent perturbative theories [19–21], for instance. In addition, it was also reached by applying semiclassical methods to quantum propagators written in the path-integral formalism, both in the position [22, 23] and coherent-state [24, 25] representations. In this case, the semiclassical formula for entanglement becomes a functional of trajectories of the corresponding classical system.

The present work can be seen as a substantial extension of Ref. [24], where one deduces a semiclassical expression for the reduced linear entropy, which is an entanglement quantifier for bipartite pure states. There, the *real* classical trajectory departing from the phase-space point defined by the center of the initial state is identified as the main ingredient to semiclassically evaluate entanglement. This approach leads to a remarkably simple final formula, which is accurate only for short values of time. By means of a case study, it was shown that the semiclassical entropy according to this theory monotonically increases with time, while its quantum counterpart has a much richer dynamical behavior; for the studied system, it is periodic, having many oscillations during a period. Here, we revisit that formalism, finding a way to include *complex* trajectories in the calculation. We point out that we do not introduce *ad-hoc* assumptions in this new theory. Effectively, an analytic continuation in clear consonance with the whole formalism — and unnoticed in Ref. [24] — is now performed, so that complex trajectories become crucial. Curiously, our new expression for entanglement depends on sets of four generally complex trajectories mutually connected through what we call *entangled boundary conditions*. Considering the same numerical example studied in Ref. [24], we also show that the inclusion of these new ingredients means extending the accuracy of the approximated formula for very long times. Surprisingly, it faithfully reproduces even the oscillations seen in the quantum result.

We organize the paper as follows. In Sect. II, we will present the basic formalism used to achieve our main result, namely, we will show the semiclassical formula for the quantum propagator in the coherent-state representation, as well as its complex conjugate, and their relation with the reduced linear entropy. Then, we will develop our semiclassical approximation in Sect. III, which basically consists in solving the integral representation of the reduced linear entropy through the steepest descent method. We will illustrate our theory by applying their

ideas to a specific Hamiltonian in Sect. IV, and, at last, some important remarks will be done in Sect. V.

II. PRELIMINARY RESULTS

In this work we are concerned with entanglement dynamics of a pure bipartite state $\hat{\rho}$ composed of the subsystems x and y. It can be quantified by the linear entropy of the reduced density matrix,

$$S_{\rm lin}(\hat{\rho}_y) = S_{\rm lin}(\hat{\rho}_x) = 1 - P(\hat{\rho}_x), \tag{1}$$

where $\hat{\rho}_{x,y} = {\rm Tr}_{y,x}\hat{\rho}$ and $\hat{\rho} = \hat{\rho}(T)$ is the time-evolved state. For the sake of simplicity, in our calculations we will focus on the time-dependent purity P_T of the reduced density matrix $\hat{\rho}_x$, defined simply by

$$P_T \equiv P(\hat{\rho}_x) = {\rm Tr}_x\{\hat{\rho}_x^2\} = {\rm Tr}_x\left\{[{\rm Tr}_y\hat{\rho}(T)]^2\right\}. \tag{2}$$

We also assume the initial *separable* state given by

$$|\mathbf{z}_0\rangle = |z_{0x}\rangle \otimes |z_{0y}\rangle, \tag{3}$$

where $|z_{0r}\rangle$ (henceforward, the subscript r can assume x or y) is a canonical one-dimensional coherent state, exhaustively studied in Refs. [26–28]. Then, considering a generic time-independent Hamiltonian $\hat{H}$, by taking the traces in Eq. (2) using the coherent-state basis, we have

$$\begin{aligned} P_T \;=\; & \int K_+((w_x^*, z_y^*), \mathbf{z}_0, T)\; K_-(\mathbf{z}_0^*, (z_x, z_y), T) \\ & \times K_+((z_x^*, w_y^*), \mathbf{z}_0, T)\; K_-(\mathbf{z}_0^*, (w_x, w_y), T) \\ & \times {\rm d}^2\mu(z_y)\; {\rm d}^2\mu(w_y)\; {\rm d}^2\mu(z_x)\; {\rm d}^2\mu(w_x), \end{aligned} \tag{4}$$

where

$${\rm d}^2\mu(z_r) \equiv \frac{{\rm d}[{\rm Re}(z_r)]{\rm d}[{\rm Im}(z_r)]}{\pi} \equiv \frac{{\rm d}z_r\; {\rm d}z_r^*}{2\pi i} \tag{5}$$

(and the equivalent for w_r), implying that integration should be done over the whole complex spaces z_x, z_y, w_x, and w_y. The quantum forward propagator K_+ and backward propagator K_- are expressed by

$$K_\pm(\mathbf{z}_\eta^*, \mathbf{z}_\mu, T) \equiv \langle \mathbf{z}_\eta | e^{\mp i\hat{H}T/\hbar} | \mathbf{z}_\mu \rangle. \tag{6}$$

Equation (4) is our starting point to perform a semiclassical approximation. Basically, the strategy is to replace the four quantum functions $K_\pm$ with their semiclassical versions, and properly evaluate the integral. We emphasize that, in the present approach, the quantum description is initially well established and, through the introduction of approximative methods, an auxiliary equivalent classical system naturally emerges. From the resulting scenario, one identifies crucial classical elements—certain complex trajectories—and deduces their contributions to the semiclassical calculation. This is exactly the essence of the semiclassical approximation for K_+, derived many years ago for canonical [29–34] and spin [35–39] degrees of freedom, and K_-, achieved and studied only recently [24, 25, 40]. In the next two subsections we simply present the useful results from these references, suggesting, in particular, Refs. [24, 32] as sources for further details.

A. Complex classical trajectories

Essentially, for both propagators defined by Eq. (6), *complex classical trajectories* are the ingredients to calculate their respective semiclassical approximations. For convenience, such trajectories are expressed in terms of unusual variables,

$$\{\mathbf{u}(t), \mathbf{v}(t)\} = \{[u_x(t), u_y(t)], [v_x(t), v_y(t)]\}. \tag{7}$$

In addition, they are governed by Hamilton's equation

$$\frac{\partial\tilde{H}}{\partial u_r} = -i\hbar\,\dot{v}_r \quad \text{and} \quad \frac{\partial\tilde{H}}{\partial v_r} = i\hbar\,\dot{u}_r, \tag{8}$$

where the classical auxiliary Hamiltonian $\tilde{H}$ is defined in terms of the expectation value of the Hamilton operator $\hat{H}$,

$$\tilde{H} \equiv \tilde{H}(\mathbf{v}, \mathbf{u}), \quad \text{with} \quad \tilde{H}(\mathbf{z}^*, \mathbf{z}) \equiv \langle \mathbf{z}|\hat{H}|\mathbf{z}\rangle. \tag{9}$$

Concerning the boundary conditions that contributing trajectories must satisfy, we point out that there exist differences between those applied to the forward propagator and those relative to the backward one:

$$\begin{aligned} &\mathbf{u}' = \mathbf{z}_\mu \quad \text{and} \quad \mathbf{v}'' = \mathbf{z}_\eta^* \quad (\text{for } K_+); \\ &\mathbf{u}'' = \mathbf{z}_\mu \quad \text{and} \quad \mathbf{v}' = \mathbf{z}_\eta^* \quad (\text{for } K_-). \end{aligned} \tag{10}$$

Here, single (double) prime refers to initial (final) time. The complex numbers $\mathbf{z}_\mu = (z_{\mu x}, z_{\mu y})$ and $\mathbf{z}_\eta^* = (z_{\eta x}^*, z_{\eta y}^*)$ are the labels of the coherent states involved in $K_\pm$, as shown in Eq. (6).

At this point, some comments are opportune. *First*, we should emphasize that Eqs. (8) to (10) completely define the trajectories to be considered in the semiclassical version of $K_\pm$ as function of their independent variables $(\mathbf{z}_\eta^*, \mathbf{z}_\mu, T)$. However, more than one trajectory may be found for a given set of these input parameters. *A priori*, all of them should be included in the calculation, as we will show later.

Second, we would like to justify why these trajectories are generically classified as *complex*. Let variables $\mathbf{u}$ and $\mathbf{v}$ be written as

$$\mathbf{u} = \frac{\mathbf{q} + i\mathbf{p}}{\sqrt{2\hbar}} \quad \text{and} \quad \mathbf{v} = \frac{\mathbf{q} - i\mathbf{p}}{\sqrt{2\hbar}}. \tag{11}$$

This choice is convenient because Hamilton's equation (8) would assume, in this case, the familiar form

$$\frac{\partial\bar{H}}{\partial q_r} = -\dot{p}_r \quad \text{and} \quad \frac{\partial\bar{H}}{\partial p_r} = \dot{q}_r, \tag{12}$$

where $\bar{H} = \tilde{H}(\mathbf{v}[\mathbf{q},\mathbf{p}],\mathbf{u}[\mathbf{q},\mathbf{p}])$. Additionally, let the coherent states $|\mathbf{z}_\mu\rangle$ and $|\mathbf{z}_\eta\rangle$ in Eq. (6) be such that

$$\mathbf{z}_\mu = \frac{\mathbf{q}_\mu + i\mathbf{p}_\mu}{\sqrt{2\hbar}} \quad \text{and} \quad \mathbf{z}^*_\eta = \frac{\mathbf{q}_\eta - i\mathbf{p}_\eta}{\sqrt{2\hbar}}. \tag{13}$$

Then, first considering only K_+ for simplicity, we conclude as follows. If $\mathbf{q}$ and $\mathbf{p}$ are real variables, $\mathbf{u}$ and $\mathbf{v}$ are complex conjugate of each other, as shown by Eq. (11). The *initial* boundary condition $\mathbf{u}' = \mathbf{z}_\mu$ of Eq. (10) would, therefore, determine completely the contributing trajectory, because it defines its initial phase space point $(\mathbf{q}',\mathbf{p}')$. In general, however, it would not naturally satisfy the final constraint $\mathbf{v}'' = \mathbf{z}^*_\eta$, given the arbitrariness of $\mathbf{z}^*_\eta$ and T. In the very *particular case* where even the final boundary condition is satisfied, such a trajectory should contribute to the evaluation of the semiclassical propagator, and it is classified as a *real trajectory*, since it lives in an ordinary real phase space $(\mathbf{q},\mathbf{p})$. Contrarily, in the general case $\mathbf{q}$ and $\mathbf{p}$ are complex variables, so that $\mathbf{u}$ and $\mathbf{v}$ are not complex conjugate of each other, and the boundary conditions are no more over-determined. Usually, Eq. (10) can be satisfied, sometimes by more than one trajectory, and the solutions are called *complex trajectories*, as they live in an extended complex phase-space $(\mathbf{q},\mathbf{p})$. The same arguments can be easily adapted to reach the same conclusion for K_-.

B. Semiclassical Propagators

The semiclassical formula for both forward and backward coherent-state quantum propagators (6) is written as

$$\mathcal{K}_\pm\left(\mathbf{z}^*_\eta,\mathbf{z}_\mu,T\right) = \sum_{\text{c.t.}} \mathcal{D}_\pm \; e^{\frac{i}{\hbar}(\mathcal{S}_\pm+\mathcal{G}_\pm)-\Lambda}, \tag{14}$$

where the sum runs over all complex classical trajectories presented in the last subsection. The complex action $\mathcal{S}_\pm = \mathcal{S}_\pm(\mathbf{z}^*_\eta,\mathbf{z}_\mu,T)$ is expressed in terms of them as

$$\frac{i}{\hbar}\mathcal{S}_\pm = \pm\int_0^T \left[\frac{1}{2}\left(\mathbf{u}\cdot\dot{\mathbf{v}} - \mathbf{v}\cdot\dot{\mathbf{u}}\right) - \frac{i}{\hbar}\tilde{H}\right]\mathrm{d}t + \tilde{\Lambda} \tag{15}$$

and the function $\mathcal{G}_\pm = \mathcal{G}_\pm(\mathbf{z}^*_\eta,\mathbf{z}_\mu,T)$ as

$$\mathcal{G}_\pm = \pm\frac{1}{2}\int_0^T \left(\frac{i}{\hbar}\frac{\partial^2\tilde{H}}{\partial u_x\partial v_x} + \frac{i}{\hbar}\frac{\partial^2\tilde{H}}{\partial u_y\partial v_y}\right)\mathrm{d}t. \tag{16}$$

The element Λ, which accounts for the normalization, is given by

$$\Lambda = \frac{1}{2}\left(\mathbf{z}^*_\eta\cdot\mathbf{z}_\eta + \mathbf{z}^*_\mu\cdot\mathbf{z}_\mu\right), \tag{17}$$

while $\tilde{\Lambda}$ [see Eq. (15)] reads

$$\tilde{\Lambda} = \frac{1}{2}\left(\mathbf{u}'\mathbf{v}' + \mathbf{u}''\mathbf{v}''\right). \tag{18}$$

Finally, we write the prefactor $\mathcal{D}_\pm$ as

$$\mathcal{D}_\pm = \left[\det\left(\frac{i}{\hbar}\mathbf{S}^{(\pm)}_{\mathbf{z}_\mu\mathbf{z}^*_\eta}\right)\right]^{1/2}, \tag{19}$$

where $\mathbf{S}^{(\pm)}_{\mathbf{z}_\mu\mathbf{z}^*_\eta}$ is the 2×2 matrix

$$\mathbf{S}^{(\pm)}_{\mathbf{z}_\mu\mathbf{z}^*_\eta} = \begin{pmatrix} \dfrac{\partial^2\mathcal{S}_\pm}{\partial z_{\mu x}\,\partial z^*_{\eta x}} & \dfrac{\partial^2\mathcal{S}_\pm}{\partial z_{\mu x}\,\partial z^*_{\eta y}} \\ \dfrac{\partial^2\mathcal{S}_\pm}{\partial z_{\mu y}\,\partial z^*_{\eta x}} & \dfrac{\partial^2\mathcal{S}_\pm}{\partial z_{\mu y}\,\partial z^*_{\eta y}} \end{pmatrix}. \tag{20}$$

Differentiating $\mathcal{S}_\pm$, we obtain results that will be important for the present work:

$$\begin{aligned} \frac{i}{\hbar}\frac{\partial\mathcal{S}_+}{\partial z_{\mu r}} &= v'_r, \qquad \frac{i}{\hbar}\frac{\partial\mathcal{S}_-}{\partial z_{\mu r}} = v''_r, \\ \frac{i}{\hbar}\frac{\partial\mathcal{S}_+}{\partial z^*_{\eta r}} &= u''_r, \qquad \frac{i}{\hbar}\frac{\partial\mathcal{S}_-}{\partial z^*_{\eta r}} = u'_r. \end{aligned} \tag{21}$$

Another important relation can be found by differentiating Eq. (21). Rearranging the expression obtained, we conclude that

$$\begin{aligned} \tfrac{i}{\hbar}\mathbf{S}^{(+)}_{\mathbf{z}_\mu\mathbf{z}^*_\eta} &= \mathbf{M}^{-1}_{\mathbf{vv}}, & \tfrac{i}{\hbar}\mathbf{S}^{(-)}_{\mathbf{z}_\mu\mathbf{z}^*_\eta} &= \mathbf{M}^{-1}_{\mathbf{uu}}, \\ \tfrac{i}{\hbar}\mathbf{S}^{(+)}_{\mathbf{z}^*_\eta\mathbf{z}^*_\eta} &= \mathbf{M}_{\mathbf{uv}}\mathbf{M}^{-1}_{\mathbf{vv}}, & \tfrac{i}{\hbar}\mathbf{S}^{(-)}_{\mathbf{z}_\mu\mathbf{z}_\mu} &= \mathbf{M}_{\mathbf{vu}}\mathbf{M}^{-1}_{\mathbf{uu}}. \end{aligned} \tag{22}$$

Quantities at the right hand sides of these equalities are 2×2 blocks of the stability matrix $\mathbf{M}$ of the respective trajectory, which is defined as

$$\begin{pmatrix}\delta\mathbf{u}''\\ \delta\mathbf{v}''\end{pmatrix} = \mathbf{M}\begin{pmatrix}\delta\mathbf{u}'\\ \delta\mathbf{v}'\end{pmatrix} = \begin{pmatrix}\mathbf{M}_{\mathbf{uu}} & \mathbf{M}_{\mathbf{uv}}\\ \mathbf{M}_{\mathbf{vu}} & \mathbf{M}_{\mathbf{vv}}\end{pmatrix}\begin{pmatrix}\delta\mathbf{u}'\\ \delta\mathbf{v}'\end{pmatrix}, \tag{23}$$

where $\delta\mathbf{u}'$ and $\delta\mathbf{v}'$ are arbitrarily small initial displacements around the classical trajectory, while $\delta\mathbf{u}''$ and $\delta\mathbf{v}''$ represent their propagation until the final time T.

III. SEMICLASSICAL LINEAR ENTROPY

We now focus on the evaluation of integral (4), replacing the quantum propagators with their semiclassical formulas (14),

$$\begin{aligned} K_+((w^*_x,z^*_y),\mathbf{z}_0,T) &\to \mathcal{K}_+((w^*_x,z^*_y),\mathbf{z}_0,T),\\ K_-(\mathbf{z}^*_0,(z_x,z_y),T) &\to \mathcal{K}_-(\mathbf{z}^*_0,(z_x,z_y),T),\\ K_+((z^*_x,w^*_y),\mathbf{z}_0,T) &\to \mathcal{K}_+((z^*_x,w^*_y),\mathbf{z}_0,T),\\ K_-(\mathbf{z}^*_0,(w_x,w_y),T) &\to \mathcal{K}_-(\mathbf{z}^*_0,(w_x,w_y),T). \end{aligned} \tag{24}$$

As it will become clear soon, it is convenient to change our notation in the following way

$$\begin{aligned} \mathcal{K}_+((w^*_x,z^*_y),\mathbf{z}_0,T) &\to \mathcal{K}_1((v''_{1x},v''_{1y}),\mathbf{z}_0,T),\\ \mathcal{K}_-(\mathbf{z}^*_0,(z_x,z_y),T) &\to \mathcal{K}_2(\mathbf{z}^*_0,(u''_{2x},u''_{2y}),T),\\ \mathcal{K}_+((z^*_x,w^*_y),\mathbf{z}_0,T) &\to \mathcal{K}_3((v''_{3x},v''_{3y}),\mathbf{z}_0,T),\\ \mathcal{K}_-(\mathbf{z}^*_0,(w_x,w_y),T) &\to \mathcal{K}_4(\mathbf{z}^*_0,(u''_{4x},u''_{4y}),T), \end{aligned} \tag{25}$$

where, induced by Eq. (10), we implicitly renamed the integration variables of (4); in what follows, functions $\mathcal{D}_j$, $\mathcal{S}_j$, and so on will be evidently related to the propagator $\mathcal{K}_j$ (for $j = 1, \ldots, 4$). Notice that the integral with these replacements involves four semiclassical propagators, each of them with possibly many contributing trajectories. To avoid this difficulty at this point, we will momentarily assume that there exists only one contribution for each propagator. Then, the semiclassical version of P_T is

$$\begin{aligned}\mathcal{P}_T \;=\; & \int \mathcal{D}_1\mathcal{D}_2\mathcal{D}_3\mathcal{D}_4\; e^{\mathcal{E}}\; \frac{\mathrm{d}u''_{2y}\;\mathrm{d}v''_{1y}}{2\pi i}\;\frac{\mathrm{d}u''_{4y}\;\mathrm{d}v''_{3y}}{2\pi i} \\ & \times \frac{\mathrm{d}u''_{2x}\;\mathrm{d}v''_{3x}}{2\pi i}\;\frac{\mathrm{d}u''_{4x}\;\mathrm{d}v''_{1x}}{2\pi i},\end{aligned} \tag{26}$$

where

$$\begin{aligned}\mathcal{E} \;=\; & \frac{i}{\hbar}\sum_{j=1,4}(\mathcal{S}_j + \mathcal{G}_j) - 2|\mathbf{z}_0|^2 \\ & - u''_{2y}v''_{1y} - u''_{4y}v''_{3y} - u''_{2x}v''_{3x} - u''_{4x}v''_{1x}.\end{aligned} \tag{27}$$

Integrating expression (26) in a straightforward way would effectively demand an enormous effort. For a given point in the set of integration variables, in general four different trajectories relative to their respective propagator should be found. Precisely, they should satisfy the following boundary conditions

$$\begin{aligned}&\mathbf{u}'_1 = \mathbf{z}_0,\;\; \mathbf{v}''_1 = (v''_{1x}, v''_{1y}),\;\; \text{for } \mathcal{K}_1((v''_{1x}, v''_{1y}), \mathbf{z}_0, T);\\ &\mathbf{v}'_2 = \mathbf{z}^*_0,\;\; \mathbf{u}''_2 = (u''_{2x}, u''_{2y}),\;\; \text{for } \mathcal{K}_2(\mathbf{z}^*_0, (u''_{2x}, u''_{2y}), T);\\ &\mathbf{u}'_3 = \mathbf{z}_0,\;\; \mathbf{v}''_3 = (v''_{3x}, v''_{3y}),\;\; \text{for } \mathcal{K}_3((v''_{3x}, v''_{3y}), \mathbf{z}_0, T);\\ &\mathbf{v}'_4 = \mathbf{z}^*_0,\;\; \mathbf{u}''_4 = (u''_{4x}, u''_{4y}),\;\; \text{for } \mathcal{K}_4(\mathbf{z}^*_0, (u''_{4x}, u''_{4y}), T);\end{aligned} \tag{28}$$

as predicted by Eq. (10). Once the four trajectories are defined, the next step is evaluating the integrand with them. Obviously, this procedure should be repeated for all points of the integration variables set, summing each contribution to evaluate $\mathcal{P}_T$.

In the present approach, instead of using the strategy mentioned above, we will solve Eq. (26) using the steepest descent method [41], in accordance with the formalism adopted to derive the semiclassical expression (14). Such a method is proper to evaluate integrals like $\int_C g(z)\exp[\lambda f(z)]\,\mathrm{d}z$ in the asymptotic limit $\lambda \to \infty$, which is similar to integral (26) for $\hbar \to 0$, except for the number of integration variables. Basically, the method consists of: finding the saddle point $\bar{z}$ of $f(z)$; changing the path of integration C in order to coincide with the steepest descents of $\bar{z}$; expanding $f(z)$ up to second order around the saddle point; and performing the remaining Gaussian integral. All these points will be done in the following, adapted to Eq. (26), except for the discussion about the possibility of deforming C, assumed here to be true. Following Ref. [41], critical points to evaluate (26) are the saddle points defined by eight equations,

$$\frac{\partial\bar{\mathcal{E}}}{\partial\bar{u}''_{2y}} = \frac{\partial\bar{\mathcal{E}}}{\partial\bar{v}''_{1y}} = \frac{\partial\bar{\mathcal{E}}}{\partial\bar{u}''_{4y}} = \ldots = \frac{\partial\bar{\mathcal{E}}}{\partial\bar{v}''_{1x}} = 0, \tag{29}$$

where the bar over the symbols stands for the critical point. As usual, derivatives of functions $\mathcal{G}_j$ are disregarded [32] in comparison with derivatives of $\mathcal{S}_j$. Thus, using Eq. (21), conditions for the saddle point become

$$\begin{aligned}&\bar{v}''_{2y} = \bar{v}''_{1y},\;\; \bar{u}''_{1y} = \bar{u}''_{2y},\;\; \bar{v}''_{4y} = \bar{v}''_{3y},\;\; \bar{u}''_{3y} = \bar{u}''_{4y},\\ &\bar{v}''_{2x} = \bar{v}''_{3x},\;\; \bar{u}''_{3x} = \bar{u}''_{2x},\;\; \bar{v}''_{4x} = \bar{v}''_{1x},\;\; \bar{u}''_{1x} = \bar{u}''_{4x}.\end{aligned} \tag{30}$$

Notice, at this point, that the saddle point definition (29) has become a prescription for contributing trajectories (30), which will be interpreted below.

Take for instance the first two equalities of Eq. (30). If we return to the original integration variables, they will become $\bar{v}''_{2y} = z^*_y$ and $\bar{u}''_{1y} = z_y$. On the other hand, from Eq. (28), we would have $\bar{u}''_{2y} = z_y$ and $\bar{v}''_{1y} = z^*_y$. It implies that $\bar{v}''_{2y}$ and $\bar{u}''_{2y}$ are complex conjugate of each other, and the same for $\bar{v}''_{1y}$ and $\bar{u}''_{1y}$. When all expressions of Eq. (30) are taken into account, by following this reasoning, we conclude that $\bar{v}''_{jr}$ and $\bar{u}''_{jr}$ are complex conjugate of each other, for any j and r. Exactly as asserted in Refs. [24, 25], it means that only *real* trajectories contribute to the calculation. Furthermore, the four trajectories can be easily proven to be the same, depending only on the initial coherent-state label $\mathbf{z}_0$,

$$\mathbf{u}' = \mathbf{z}_0 \quad \text{and} \quad \mathbf{v}'' = \mathbf{z}^*_0 \quad \text{(real trajectory)}.$$

At this point, the present work takes a different route from that of Refs. [24, 25]. Instead of returning to the original integration variables, we will interpret Eq. (30) as they are presented. Effectively, it is equivalent to treat z_r and z^*_r (the same for w_r and w^*_r) as independent variables, strategy which is in clear consonance with the approach used to deduce Eq. (14). In fact, from this reasoning, Eq. (30) together with Eq. (28) finally establish the conditions for the critical trajectories involved in $\mathcal{P}_T$

$$\begin{aligned}&\bar{\mathbf{u}}'_1 = \mathbf{z}_0,\;\; \bar{\mathbf{v}}''_1 = (\bar{v}''_{1x}, \bar{v}''_{1y}),\;\; \text{and}\;\; \bar{\mathbf{u}}''_1 = (\bar{u}''_{4x}, \bar{u}''_{2y});\\ &\bar{\mathbf{v}}'_2 = \mathbf{z}^*_0,\;\; \bar{\mathbf{u}}''_2 = (\bar{u}''_{2x}, \bar{u}''_{2y}),\;\; \text{and}\;\; \bar{\mathbf{v}}''_2 = (\bar{v}''_{3x}, \bar{v}''_{1y});\\ &\bar{\mathbf{u}}'_3 = \mathbf{z}_0,\;\; \bar{\mathbf{v}}''_3 = (\bar{v}''_{3x}, \bar{v}''_{3y}),\;\; \text{and}\;\; \bar{\mathbf{u}}''_3 = (\bar{u}''_{2x}, \bar{u}''_{4y});\\ &\bar{\mathbf{v}}'_4 = \mathbf{z}^*_0,\;\; \bar{\mathbf{u}}''_4 = (\bar{u}''_{4x}, \bar{u}''_{4y}),\;\; \text{and}\;\; \bar{\mathbf{v}}''_4 = (\bar{v}''_{1x}, \bar{v}''_{3y}).\end{aligned} \tag{31}$$

Notice that the final coordinates of the four trajectories are mutually connected. That is, $\bar{v}''_{1x} = \bar{v}''_{4x}$, $\bar{v}''_{1y} = \bar{v}''_{2y}$, and so on. In this sense, we say that the semiclassical linear entropy depends on sets of four trajectories with *entangled boundary conditions* at the final time. Clearly, the set of four real trajectories described above also satisfies conditions (31), and should be included in the calculation. We emphasize that these boundary conditions are by no means inserted by hand in the theory. They naturally arise from the application of the steepest descent method on integral (26), provided that we allow a proper analytic continuation, as discussed above. At last, we point out that this result is achieved without assuming any consideration concerning the Hamiltonian.

With the conditions of critical trajectories well defined, we assume that solutions of Eq. (31) can be generally

found, and proceed with the evaluation of integral (26). Following Ref. [41], we should expand the integrand up to second order around the parameters of the critical set of trajectories. Actually, as rigorously discussed in Ref. [32], the expansion is not performed for functions $\mathcal{G}_j$ and prefactors $\mathcal{D}_j$. They are simply evaluated at the saddle point, without harming the accuracy of the approximation. We get

$$\mathcal{P}_T \;=\; \sum_{\text{sets}} \bar{\mathcal{D}}_1\; \bar{\mathcal{D}}_2\; \bar{\mathcal{D}}_3\; \bar{\mathcal{D}}_4\; e^{\bar{\mathcal{E}}}\; \mathcal{I}. \tag{32}$$

The sum spans all sets of critical trajectories and naturally encompasses the hitherto neglected sum of Eq. (14). Also,

$$\mathcal{I} \;=\; \int \exp\left\{\frac{1}{2}\delta\mathbf{r}^t\,\bar{\mathbf{A}}\;\delta\mathbf{r}\right\}\;\frac{\mathrm{d}[\delta u''_{2y}]\;\mathrm{d}[\delta v''_{1y}]}{2\pi i} \times \frac{\mathrm{d}[\delta u''_{4y}]\;\mathrm{d}[\delta v''_{3y}]}{2\pi i}\;\frac{\mathrm{d}[\delta u''_{2x}]\;\mathrm{d}[\delta v''_{3x}]}{2\pi i}\;\frac{\mathrm{d}[\delta u''_{4x}]\;\mathrm{d}[\delta v''_{1x}]}{2\pi i}, \tag{33}$$

where $\delta\mathbf{r}^t$ (t stands for transpose) is a line vector containing the new integration variables ordered in a specific way,

$$\delta\mathbf{r}^t \equiv \left(\delta v''_{1x},\, \delta v''_{1y},\, \delta u''_{2x},\, \delta u''_{2y},\, \delta v''_{3x},\, \delta v''_{3y},\, \delta u''_{4x},\, \delta u''_{4y}\right),$$

with $\delta v''_{1x} \equiv (v''_{1x} - \bar{v}''_{1x})$, $\delta v''_{1y} = (v''_{1y} - \bar{v}''_{1y})$, and so on. We now present the matrix

$$\bar{\mathbf{A}} = \begin{pmatrix} \frac{i}{\hbar}\bar{\mathbf{S}}^{(1)}_{\mathbf{v}''\mathbf{v}''} & -\mathbf{1}_y & 0 & -\mathbf{1}_x \\ -\mathbf{1}_y & \frac{i}{\hbar}\bar{\mathbf{S}}^{(2)}_{\mathbf{u}''\mathbf{u}''} & -\mathbf{1}_x & 0 \\ 0 & -\mathbf{1}_x & \frac{i}{\hbar}\bar{\mathbf{S}}^{(3)}_{\mathbf{v}''\mathbf{v}''} & -\mathbf{1}_y \\ -\mathbf{1}_x & 0 & -\mathbf{1}_y & \frac{i}{\hbar}\bar{\mathbf{S}}^{(4)}_{\mathbf{u}''\mathbf{u}''} \end{pmatrix},$$

where

$$\mathbf{1}_x = \begin{pmatrix} 1 & 0 \\ 0 & 0 \end{pmatrix}, \qquad \mathbf{1}_y = \begin{pmatrix} 0 & 0 \\ 0 & 1 \end{pmatrix},$$

and the 2×2 blocks in the diagonal of $\bar{\mathbf{A}}$ are defined in analogy to Eq. (20), and can be written in terms of the tangent matrix $\mathbf{M}$ according to Eq. (22).

Our last step to reach an expression for quantum entanglement in terms of classical ingredients is to solve integral $\mathcal{I}$, which is simply a Gaussian integral [32], whose result is $1/\sqrt{\det\bar{\mathbf{A}}}$. Finally, the linear entropy (1) can be semiclassically expressed as

$$\mathcal{S}_{\text{lin}} \;=\; 1 - \sum_{\text{sets}} \frac{\mathcal{D}_1\;\mathcal{D}_2\;\mathcal{D}_3\;\mathcal{D}_4\;e^{\mathcal{E}}}{\sqrt{\det\mathbf{A}}}. \tag{34}$$

This is our final formula. Notice that we removed the bars over the functions for the sake of clearness. We emphasize that sets of four trajectories contributing to $\mathcal{S}_{\text{lin}}$ should satisfy the *entangled boundary conditions* (31). Once these trajectories are determined, all functions involved in Eq. (34) can be evaluated. In the following, we will check for a particular system that, although the set of real trajectories is inefficient to accurately describe entanglement for longer values of time [24], the inclusion of *a few sets* of complex trajectories, as prescribed by (34), leads to excellent results.

IV. APPLICATION

In this section we will apply the present formalism to the same physical system used in Ref. [24]. Our intention is to show that the improvement performed on that theory gives rise to semiclassical results in excellent agreement with the full quantum calculation, even for very long values of time.

The Hamiltonian to be studied is given by

$$\hat{H} = \hat{H}_x \otimes \mathbf{1}_y + \mathbf{1}_x \otimes \hat{H}_y + \lambda \hat{H}_x \otimes \hat{H}_y, \tag{35}$$

where

$$\hat{H}_r = \frac{\hat{p}_r^2}{2m_r} + \frac{m_r\omega_r^2\hat{q}_r^2}{2} \tag{36}$$

refers to the harmonic oscillator system. For our purposes, we will assume the initial state as the coherent state $|\mathbf{z}_0\rangle = |z_{0x}\rangle \otimes |z_{0y}\rangle$, where $|z_{0r}\rangle$ is associated to $\hat{H}_r$. In this scenario, we remind that the label of the initial coherent state can be written in terms of

$$z_{0r} = \frac{1}{\sqrt{2}}\left(\frac{q_{0r}}{b_r} + \frac{ip_{0r}}{c_r}\right), \tag{37}$$

where the pair (q_{0r}, p_{0r}) gives the center of the wave packet $|\mathbf{z}_0\rangle$ in phase space, and (b_r, c_r) its respective uncertainties.

In terms of the annihilation and creation operators,

$$\hat{a}_r = \frac{1}{\sqrt{2}}\left(\frac{\hat{q}_r}{b_r} + \frac{i\hat{p}_r}{c_r}\right) \;\text{ and }\; \hat{a}_r^\dagger = \frac{1}{\sqrt{2}}\left(\frac{\hat{q}_r}{b_r} - \frac{i\hat{p}_r}{c_r}\right),$$

respectively, with

$$b_r = \sqrt{\frac{\hbar}{m_r\omega_r}} \quad\text{and}\quad c_r = \sqrt{m_r\hbar\omega_r},$$

the Hamiltonian becomes

$$\hat{H} = \hbar\Omega_x\hat{a}_x^\dagger\hat{a}_x + \hbar\Omega_y\hat{a}_y^\dagger\hat{a}_y + \hbar\Gamma\hat{a}_x^\dagger\hat{a}_x\,\hat{a}_y^\dagger\hat{a}_y + \epsilon_0, \tag{38}$$

where

$$\Omega_r = \omega_r + \frac{\Gamma}{2}, \quad \Gamma = \lambda\hbar\omega_x\omega_y, \quad\text{and}\quad \epsilon_0 = \frac{\hbar}{2}(\omega_x + \omega_y).$$

The linear entropy (1) of the reduced density matrix for this system can be straightforwardly evaluated, resulting in

$$S_{\text{lin}} = 1 - P_T, \tag{39}$$

where

$$P_T = e^{-2|z_{0x}|^2}\sum_{n,m}\frac{|z_{0x}|^{2(n+m)}}{n!m!}\;e^{-4|z_{0y}|^2\sin^2\left[\frac{\Gamma T(n-m)}{2}\right]}.$$

Equation (39) reveals that the entanglement dynamics for this particular system is periodic, with period given by $T_{\text{r}} \equiv 2\pi/\Gamma$, named as *recoherence time*. It can be easily checked that $S_{\text{lin}}(T = jT_{\text{r}}) = 0$, for $j = 0, 1, \ldots$. For

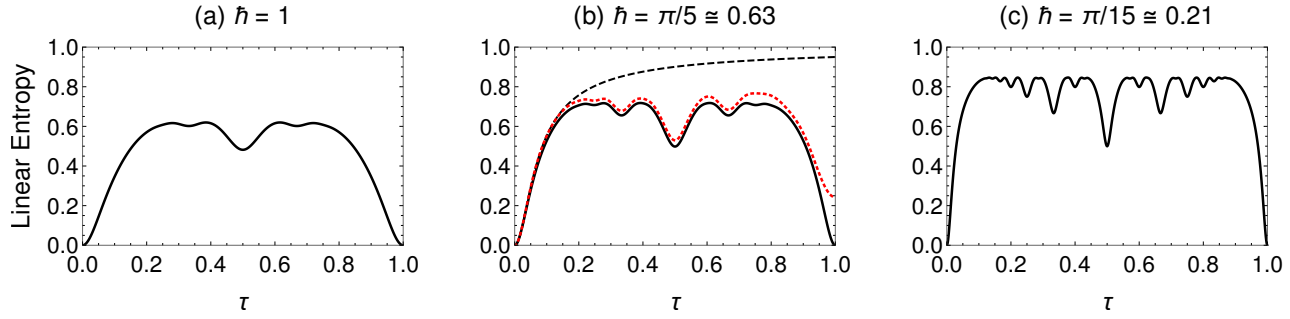

FIG. 1. Black solid lines represent quantum linear entropy of the reduced state (39) as function of the dimensionless time τ, for (a) $\hbar = 1$, (b) $\hbar = \pi/5$, and (c) $\hbar = \pi/15$. Other numerical parameters are $E_{0r} = \omega_{0r} = \lambda = 1$ and $z_{0r} = \sqrt{E_{0r}/(\hbar\omega_r)}$. In panel (b), the black dashed curve shows the contribution of the set of real trajectories to $\mathcal{S}_{\rm lin}$, while the red dotted one presents the equivalent result when a few sets of complex trajectories are considered.

this reason, in what follows, we will adopt the dimensionless time

$$\tau \equiv \frac{T}{T_{\rm r}} = \frac{\Gamma T}{2\pi}, \tag{40}$$

and restrict our study to the interval $0 \leq \tau < 1$. Notice that all the dynamics is present in this range.

Numerical parameters for the present application were chosen according to the following reasoning. The label of the initial state $|\mathbf{z}_0\rangle$ is such that

$$|z_{0r}|^2 = \frac{1}{\hbar\omega_r}\left(\frac{p_r^2}{2m_r} + \frac{m_r\omega_r^2 q_r^2}{2}\right) \equiv \frac{E_{0r}}{\hbar\omega_r}, \tag{41}$$

which, roughly speaking, suggests that, to reach a semiclassical regime, the harmonic oscillator energy E_{0r} should be much larger than $\hbar\omega_r$. Then, we hold $E_{0r} = \omega_{0r} = \lambda = 1$ and define, for simplicity, $z_{0r} = \sqrt{E_{0r}/(\hbar\omega_r)} = \hbar^{-1/2}$, meaning that z_{0r} is numerically equivalent to $\hbar^{-1/2}$. By decreasing $\hbar$ from 1, we formally go, in principle, from quantum to semiclassical limit. Besides, concerning the physical time-scale related to T, we notice that the harmonic oscillator period now is $T_{\rm ho} \equiv 2\pi/\omega_r = 2\pi$ and the recoherence time is $T_{\rm r} = T_{\rm ho}/\hbar$. Then, decreasing $\hbar$ means increasing $T_{\rm r}$.

We have, therefore, the following dilemma. If we take $\hbar = 1$, for instance, although the semiclassical regime is not achieved, the entanglement dynamics during a cycle is simple because it lasts a short time, equivalent to only one period of the harmonic oscillator. On the other hand, by taking very small values of $\hbar$, the semiclassical regime can be reached, but $T_{\rm r}$ can be much larger and the dynamics much more evolved. Figure 1 clearly illustrates this discussion, while it shows (black solid line) the behavior of $S_{\rm lin}$ as function of τ, during a whole cycle, for three values of $\hbar$: approximately 1.0, 0.63, and 0.21 for Figs. 1(a), 1(b), and 1(c), respectively. Inversely, for each plot, the recoherence time increases: 2π, 10, and 30, respectively. Thus, as we intend to semiclassically study a complete cycle $T_{\rm r}$, we cannot adopt very small values of $\hbar$, neither the largest ones, so that, in the next calculations, we will use $\hbar = \pi/5 \approx 0.63$, the value used in Fig. 1(b).

A. Auxiliary Dynamics

In order to evaluate the semiclassical version of Eq. (39), we need an underlying classical Hamiltonian, which, according to our prescription (9), is

$$H(\mathbf{v},\mathbf{u}) = \hbar\Omega_x v_x u_x + \hbar\Omega_y v_y u_y + \hbar\Gamma v_x u_x\, v_y u_y + \epsilon_0. \tag{42}$$

The classical trajectories can be readily integrated according to Eq. (8). In terms of the initial coordinates u'_x, v'_x, u'_y, and v'_y, they are

$$\begin{pmatrix} u_x(t) \\ u_y(t) \\ v_x(t) \\ v_y(t) \end{pmatrix} = \begin{pmatrix} u'_x e^{-\lambda_x t} \\ u'_y e^{-\lambda_y t} \\ v'_x e^{+\lambda_x t} \\ v'_y e^{+\lambda_y t} \end{pmatrix}, \tag{43}$$

where $\lambda_x = i\left(\Omega_x + \Gamma u'_y v'_y\right)$ and $\lambda_y = i\left(\Omega_y + \Gamma u'_x v'_x\right)$. The tangent matrix (23) can be evaluated by differentiating the last equation, so that

$$\begin{pmatrix} \delta u''_x \\ \delta u''_y \\ \delta v''_x \\ \delta v''_y \end{pmatrix} = \mathrm{M}_B\mathrm{M}_A \begin{pmatrix} \delta u'_x \\ \delta u'_y \\ \delta v'_x \\ \delta v'_y \end{pmatrix}, \tag{44}$$

where

$$\mathrm{M}_A = \begin{pmatrix} 1 & -au'_x v'_y & 0 & -au'_x u'_y \\ -au'_y v'_x & 1 & -au'_y u'_x & 0 \\ 0 & av'_x v'_y & 1 & av'_x u'_y \\ av'_y v'_x & 0 & av'_y u'_x & 1 \end{pmatrix}, \tag{45}$$

with $a = i\Gamma T$ and

$$\mathrm{M}_B = \begin{pmatrix} e^{-\lambda_x T} & 0 & 0 & 0 \\ 0 & e^{-\lambda_y T} & 0 & 0 \\ 0 & 0 & e^{+\lambda_x T} & 0 \\ 0 & 0 & 0 & e^{+\lambda_y T} \end{pmatrix}. \tag{46}$$

From these classical results, we need to identify the trajectories contributing to the semiclassical formula (34).

B. Contributing trajectories

Each term in the sum of Eq. (34) involves four trajectories. All of them have the form presented above (43), one differing from each other exclusively through their boundary conditions. Initial boundary conditions of Eq. (31) simply imply that $u'_{1r} = u'_{3r} = z_{0r}$ and $v'_{2r} = v'_{4r} = z^*_{0r}$. Final constraints, on the other hand, are more evolved. In the present application, in terms of the dimensionless time τ, they can be written as

$$\begin{aligned} e^{-ia_y(y_1-y_4)\tau} &= x_4, & e^{-ia_x(x_1-x_2)\tau} &= y_2, \\ e^{+ia_y(y_2-y_3)\tau} &= x_3, & e^{+ia_x(x_2-x_1)\tau} &= y_1, \\ e^{-ia_y(y_3-y_2)\tau} &= x_2, & e^{-ia_x(x_3-x_4)\tau} &= y_4, \\ e^{+ia_y(y_4-y_1)\tau} &= x_1, & e^{+ia_x(x_4-x_3)\tau} &= y_3, \end{aligned} \tag{47}$$

where $a_x = 2\pi\,|z_{0x}|^2$, $a_y = 2\pi\,|z_{0y}|^2$, and

$$\begin{aligned} v'_{1x} &= x_1 z^*_{0x}, & u'_{2x} &= x_2 z_{0x}, & v'_{3x} &= x_3 z^*_{0x}, & u'_{4x} &= x_4 z_{0x}, \\ v'_{1y} &= y_1 z^*_{0y}, & u'_{2y} &= y_2 z_{0y}, & v'_{3y} &= y_3 z^*_{0y}, & u'_{4y} &= y_4 z_{0y}. \end{aligned} \tag{48}$$

Manipulating Eq. (47) allows us to write the following transcendental equation for x_2,

$$x_2 = e^{+ia_y\tau\left[e^{+ia_x\left(x_2-\frac{1}{x_2}\right)\tau}-e^{-ia_x\left(x_2-\frac{1}{x_2}\right)\tau}\right]}. \tag{49}$$

Once we have found solutions for x_2, other variables can be solved as

$$\begin{aligned} y_2 &= e^{+ia_x\left(x_2-\frac{1}{x_2}\right)\tau}, \quad x_3 = x_2, \quad y_1 = y_2, \\ x_1 &= x_4 = \frac{1}{x_2}, \quad y_3 = y_4 = \frac{1}{y_2}, \end{aligned} \tag{50}$$

completing [see Eq. (48)] all the information needed to define the set of contributing trajectories. For practical reasons, to deal with this problem, we define the function

$$f(x_2) = x_2 - e^{+ia_y\tau\left[e^{+ia_x\left(x_2-\frac{1}{x_2}\right)\tau}-e^{-ia_x\left(x_2-\frac{1}{x_2}\right)\tau}\right]}, \tag{51}$$

so that finding solutions of Eq. (49) is equivalent to finding roots of $f(x_2)$.

At this point, notice that the crucial point of our application is the search for solutions of points where $f(x_2) = 0$. We will show that, except for $\tau = 0$, where only one solution exists, there are infinitely many values of x_2 satisfying this equation. As already explained, each solution gives origin to a set of four trajectories which, in principle, contributes to the value of $\mathcal{S}_{\rm lin}$.

When $\tau = 0$, the only root of $f(x_2)$ is straightforwardly found: $x_2 = 1$, which clearly gives origin to the set of real trajectories starting at $\mathbf{u}'_j = \mathbf{z}_0$ and $\mathbf{v}'_j = \mathbf{z}^*_0$, for $j = 1, 2, 3$, and 4 [see Eq. (48)]. Besides, notice that the point $x_2 = 1$ is a root, whatever is the value of τ. Keeping only this set of contributing trajectories is therefore equivalent to the approach of Ref. [24]. In Fig. 1(b) we show (black dashed line) this specific contribution to our numerical example. Notice that, as expected, it gives accurate results only for short values of time. When time runs, oscillations seen in the quantum curve are not reproduced by the real trajectory.

Another important consideration should be done. A simple inspection in Eq. (51) reveals that, if $x_2 = w$ is a complex root, then w^*, $1/w$, and $1/w^*$ are also roots of $f(x_2)$. As a consequence, we will look for roots lying only at the unitary circle of the x_2-complex plane, or outside it, and restricted to $\mathrm{Im}[x_2] \geq 0$, simplifying this root search problem. Obviously, roots lying exactly over the unitary circle (or the real axis) do not follow exactly that rule; if $|w| = 1$ (or $\mathrm{Im}[w] = 0$), then only w and w^* (or $1/w$) are roots.

Finally, in Fig. 2 we graphically look for the roots of $f(x_2)$ in the x_2-complex plane. For all plots, black solid lines delimit the unitary circle. For the reason mentioned above, no new information can be found inside this circle, then nothing is shown there. Exceptions are Fig. 2(h) and Fig. 2(i) where contour lines inside the circle are plotted for a better understanding of their structure. In addition, dashed lines refer to the curves where $\mathrm{Im}[f(x_2)] = 0$, while the dotted ones indicate those where $\mathrm{Re}[f(x_2)] = 0$. Roots of $f(x_2)$ are evidently given by intersections of dashed and dotted lines.

In Fig. 2(a), plotted for $\tau = 0$, we see that there is only one root at $x_2 = 1$. According to Fig. 2(b) to Fig. 2(e), when τ increases, some structures coming from distant regions rapidly approach the origin, bringing a large number of new roots with them. Actually, the intersection points are barely seen in Fig. 2(d) and Fig. 2(e) because they are much close to each other. However, they are there as demonstrated by Fig. 2(f) to Fig. 2(l), where magnified regions of Fig. 2(e) are plotted, showing its details in the vicinity of the real axis.

Figure 2(e) shows the scenario for $\tau = 0.333$, one third of the recoherence time $T_{\rm r}$, where the quantity of roots seems to be intractable. Among so many solutions, it is practically mandatory to get a criteria to select the relevant points. Considering that the set of real trajectories, represented by $x_2 = 1$, is enough to reproduce the quantum linear entropy for sufficiently short values of time, and given that other unimportant roots lie in remote regions in this case, it seems reasonable to neglect, at a first attempt, intersection points which are not close to the real axis. This is the motivation to plot, in Fig. 2(f) to Fig. 2(l), magnified regions of Fig. 2(e) around the real axis. Actually, they show details of its three structures positioned at the left of the origin [Figs. 2(f) to Fig. 2(h)] and other four ones located at the right of this point [Figs. 2(i) to Fig. 2(l)]. These seven structures are named St_1, St_2, ..., St_7 for convenience, as shown in each plot. From them we effectively start the selection of the contributing sets of complex trajectories, as explained in the following.

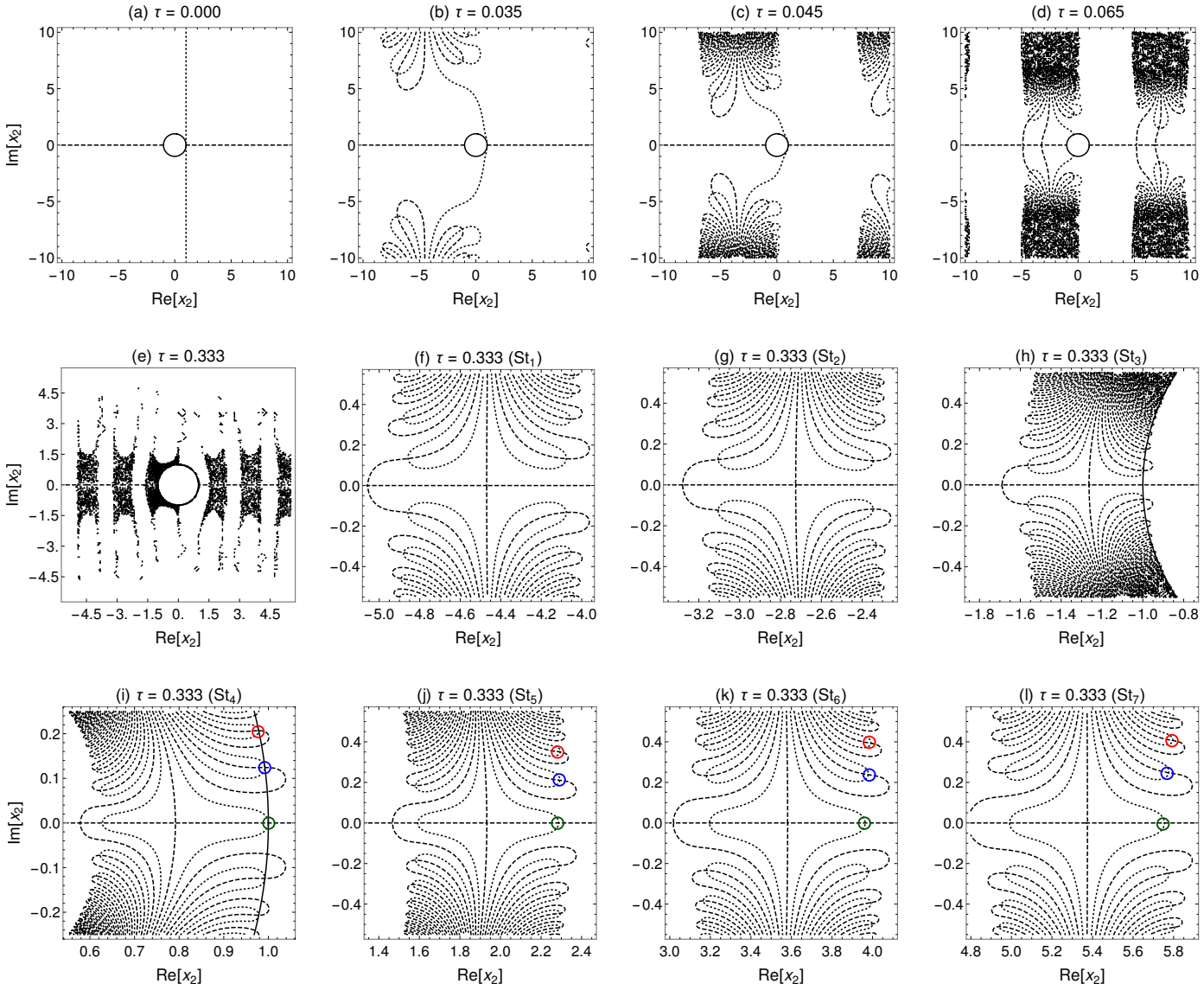

FIG. 2. Searching roots of $f(x_2)$ in the x_2-complex plane. For all plots, curves where $\mathrm{Im}[f(x_2)] = 0$ ($\mathrm{Re}[f(x_2)] = 0$) are shown by dashed (dotted) lines and the unitary circle is represented by the solid line. Intersections of dashed and dotted curves are the roots of $f(x_2)$. From panel (a) to (e), values of the dimensionless time τ assume 0, 0.035, 0.045, 0.065, and 0.333, respectively. Panels (f) to (l) are magnified regions of panel (e), showing details of its seven structures around the real axis. Green, blue, and red circles present at panels (i) to (l) identify the relevant roots for the evaluation of $\mathcal{S}_{\mathrm{lin}}$. Other numerical parameters are $E_{0r} = \omega_{0r} = \lambda = 1$, $\hbar = \pi/5$, and $z_{0r} = \sqrt{E_{0r}/(\hbar\omega_r)}$.

C. Semiclassical Results

We first emphasize that, for the whole process of finding sets of trajectories effectively contributing to $\mathcal{S}_{\mathrm{lin}}$, we only inspected the plots of Fig. 2(f) to Fig. 2(l). Even for different values of τ, there is no need to find new roots of $f(x_2)$ *graphically*. From a single root found for $\tau = 0.333$, for instance, we have iteratively got a *family* of roots associated to this solution for the whole range $0 < \tau \leq 1$, by means of a proper *numerical* procedure based on the Newton-Raphson method.

Numerically, we verified that most of the families associated with the roots seen in Fig. 2(f) to Fig. 2(l) gives origin to contributions to $\mathcal{S}_{\mathrm{lin}}$ which are negligible for any value of τ. Then, they are simply disregarded. Actually, those intersections identified by colored circles in Fig. 2(i) to Fig. 2(l) are the roots responding for relevant contributions, i.e., only the analysis of structures St_4 to St_7 produced useful results. In Fig. 3(a), for instance, we show the effects of including families of the three marked roots of Fig. 2(i). As already discussed, the point identified by the green circle is that associated with the set of real trajectories; its contribution is given by the green solid line. If we include to this result the

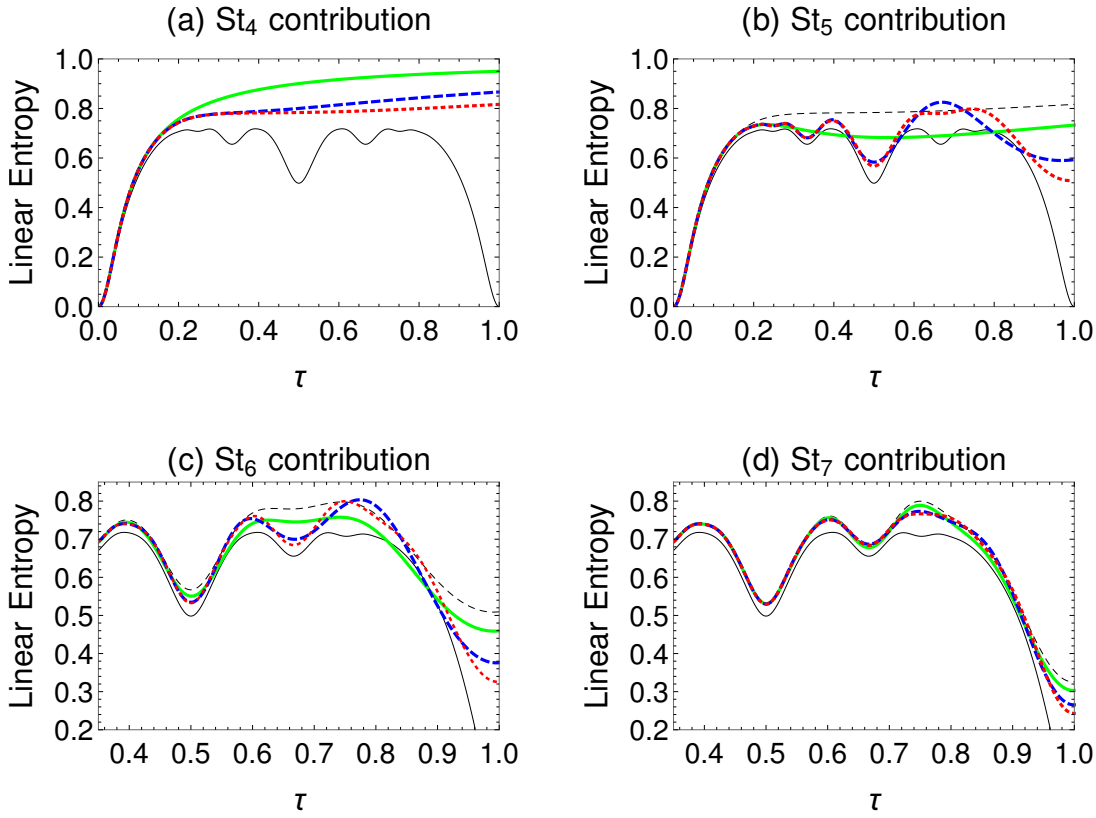

FIG. 3. Black solid lines represent the quantum linear entropy of the reduced state (39) as function of the dimensionless time τ. Numerical parameters are chosen to be the same of those of Fig. 1(b). In panel (a), the solid green line refers to $\mathcal{S}_{\rm lin}$, calculated using exclusively the set of real trajectories, associated with the root inside the green circle of Fig. 2(i); including trajectories associated with the root marked by the blue circle of Fig. 2(i) produces the blue dashed curve; and, including contributions related to the root marked by the red circle of Fig. 2(i) generates the red dotted curve. Colored lines of panels (b), (c), and (d) are built analogously to panel (a); by adding contributions to the semiclassical approach presented in Fig. 2(j), Fig. 2(k), and Fig. 2(l), respectively. Black dashed lines in panels (b), (c), and (d) are the most complete curve of the preceding panel, i.e., the red dotted curve of panels (a), (b), and (c), respectively.

family associated with the root inside the blue circle of Fig. 2(i), we get the blue dashed curve of Fig. 3(a). Still, adding the root marked by the red circle, the red dotted curve is obtained. Clearly, the inclusion of new sets of complex trajectories improves $\mathcal{S}_{\rm lin}$ based only on real trajectories. However, oscillations presented in the fully quantum linear entropy (black solid curves of Fig. 3) are still not reproduced.

Only when the highlighted roots of Fig. 2(j) are considered, the oscillatory behavior of $S_{\rm lin}$ starts to be mimetized by the semiclassical approach. In Fig. 3(b), we first add the family of the root marked by the green circle of St_5, getting the green solid line, which does not show oscillations but improves the approximation. Then, we include the root inside the blue circle and arrive at the blue dashed curve which shows a very good semiclassical result, oscillating in accordance to the quantum result until $\tau \approx 0.5$. At last, we show that including the family of the root marked by the red circle produces improvement only in the second half of the recoherence time (red dotted line).

Following the same procedure, we show in Fig. 3(c) and Fig. 3(d) the improvement gained by including roots highlighted in structures St_6 and St_7 [Fig. 2(k) and Fig. 2(l)], respectively. Now, $\mathcal{S}_{\rm lin}$ practically remains unchanged for $\tau < 0.5$. On the other hand, for $\tau > 0.5$, the semiclassical approximation becomes progressively better. When structure St_7 is considered, it can be seen that $\mathcal{S}_{\rm lin}$ is practically improved only for $\tau > 0.9$. In order to analyze our final result, we return to Fig. 1(b), where the exact $S_{\rm lin}$ is plotted (black solid line) together with the semiclassical $\mathcal{S}_{\rm lin}$ in two cases: when only real trajectories are included (black dashed line) and when complex trajectories associated to marked intersections of Fig. 2(i) to Fig. 2(l) enter in the calculation (red dotted line). Surprisingly, the inclusion of only a few sets of complex trajectories is enough to reproduce the fully quantum result during almost the whole period $T_{\rm r}$.

V. FINAL REMARKS

The present paper essentially revisits the theory presented in Ref. [24], and substantially improves its accuracy. In the adopted approach, we start from an integral expression for the linear entropy $S_{\rm lin}$ of the reduced density matrix of a pure bipartite system, initially prepared in a product of coherent states [Eqs. (1) to (4)], developing it by means of semiclassical approximations based on the steepest descent method. According to this treatment, a semiclassical formula for $S_{\rm lin}$ is written in terms of sets of four correlated trajectories of an underlying classical system (34). With respect to Ref. [24], our novelty is to consider complex trajectories in the approach. We should comment that the present contribution involves a prescription, rigorously deduced from the theory, in order to identify such trajectories.

While the contribution of real trajectories to $\mathcal{S}_{\rm lin}$ is able to reproduce the short-time behavior of its quantum counterpart $S_{\rm lin}$, we have verified for a particular system that only a few sets of complex trajectories are enough to produce accurate results even for very long values of time [these results are summarized in Fig. 1(b)]. We emphasize that a contributing set of trajectories is characterized by the *entangled boundary conditions* (31). It is worth to point out that our approach is completely different from the entangled trajectory molecular dynamics method [16, 42]. Differently from our formalism where trajectories are entangled by means of final-time boundary conditions, in Refs. [16, 42] classical dynamics is entangled due to the inclusion of a non-local term in its equations of motion, a procedure similar to that used on Bohmian quantum mechanics. Problems of interest attacked by the entangled trajectory molecular dynamics method are typical of the chemical physics field, in which the inclusion of quantum correlation phenomena has attracted considerable attention [43]. We expected that the theory presented here can also contribute to this area, however this theme is beyond the scope of the present paper.

Still referring to the set of contributing trajectories, we remind that there are important works in the literature based on the semiclassical time-evolution of the Wigner function (and its Fourier conjugate) [44–46], whose approaches also identify sets of connected trajectories entering in the calculation. The difference, in these cases, is that they deal with pairs of trajectories, instead of four, and their boundary conditions do not explicitly involve constraints among different parts (x and y, in our case) of the system, as shown in Eq. (31). Writing the linear entropy in terms of the Wigner function is possible [16], however further integrations should be done. Possibly, this procedure would connect two pairs of trajectories resulting in boundary conditions comparable to ours.

It is quite instigating to speculate about the conceptual role of the extended phase-space, which shelters the contributing trajectories. By recognizing that there are other works in different contexts clearly confirming that genuinely quantum behaviors are reproduced by semiclassical approaches only when complex trajectories are included [47–49], one wonders if the complex-extension procedure is a determinant factor to distinguish classical and quantum correlations. To develop this idea, supported by Refs. [11, 20], we first point out that the short-time entanglement can be described by classical mechanisms based on the Liouvillian theory. For greater values of time, on the other hand, no real classical strategy seems to be able to mimic entanglement, corroborating its quantum nature. The expedient used here to overcome this evident semiclassical difficulty is to extend the real phase-space to a complex one. This, therefore, suggests that classical correlations in an extended phase-space [50], a valid interpretation of boundary conditions (31), are closely related to genuinely quantum correlations. Notice that, in this case, in principle, sets of trajectories defined here could be used to describe entanglement in other possibly classical approaches. However, their complex nature seems to be unavoidable.

As far as we know, the present work is the first to define specific properties of a classical system, given by Eq. (31), which somehow carry information about quantum entanglement. Contrarily to other works which sum contributions over an ensemble of trajectories (e.g., Refs [14, 16]), our approach allowed us to identify only a few classical trajectories relevant to mimic, to a certain extent, the quantum behavior. We also understand that the announced entangled boundary conditions may encapsulate useful information to better explain the connection between the classical dynamical properties and the growth of entanglement, or, in other words, to investigate classical mechanisms associated to entanglement. By the way, some authors have recently questioned the well accepted conclusions pointing to a direct relation between chaos and rapid growth of entanglement [9, 13, 17, 18]. We consider that our work may shed some light over this discussion, but it is an issue that we intend to develop in a future work where we will also extend the formalism to spin degrees of freedom.

At last, we would like to apply the present approach to the scenario of Bell-type inequalities, in the same spirit of Ref. [52]. Since we have got an excellent reproduction of the quantum entanglement behavior by means of classical elements, we wonder if it could violate those inequalities. In the positive case, to be consistent with Bell's work, an amount of non-locality should be identified in the formalism.

ACKNOWLEDGMENTS

This study was financed in part by: Coordenação de Aperfeiçoamento de Pessoal de Nível Superior – Brasil (CAPES) — Finance Code 001; Conselho Nacional de Pesquisa – Brasil (CNPq); and Instituto Nacional de Ciência e Tecnologia/Informação Quântica – Brasil (INCT-IQ, 465469/2014-0). We also would like to thank

R. M. Angelo and F. Parisio for helpful discussions.

[1] M. A. Nielsen and I. L. Chuang, *Quantum computation and quantum information* (Cambridge University Press, U.K., 2000).
[2] R. Horodecki, P. Horodecki, M. Horodecki, and K. Horodecki, Rev. Mod. Phys. **81**, 865 (2009).
[3] M. C. Gutzwiller, *Chaos in Classical and Quantum Mechanics* (Springer-Verlag, New York, 1990).
[4] M. Brack and R. Bhaduri, *Semiclassical Physics* (Westview Press, Oxford, 2003).
[5] K. Furuya, M. C. Nemes, and G. Q. Pellegrino, Phys. Rev. Lett. **80**, 5524 (1998).
[6] S. Ghose and B. C. Sanders, Phys. Rev. A **70**, 062315 (2004).
[7] L. F. Santos, G. Rigolin, and C. O. Escobar, Phys. Rev. A **69** 042304 (2004).
[8] M. Novaes, Ann. Phys. **318**, 308 (2005).
[9] M. Lombardi and A. Matzkin, Laser Phys. **20**, 1215 (2010).
[10] C. Neil *et al*, Nature Phys. **12**, 1037 (2016).
[11] R. M. Angelo, S. A. Vitiello, M. A. M. de Aguiar, and K. Furuya, Physyca A **338**, 458 (2004).
[12] H. Han and P. Brumer, J. Phys. B **40**, S209 (2007).
[13] M. Lombardi and A. Matzkin, Phys. Rev. E **83**, 016207 (2011).
[14] G. Casati, I. Guarneri, and J. Reslen, Phys. Rev. E **85**, 036208 (2012).
[15] C. T. Asplund and D. Berenstein, Ann. Phys. **366**, 113 (2016).
[16] F. Xu, C. C. Martens, and Y. Zheng, Phys. Rev. A **96**, 022138 (2017).
[17] J. B. Ruebeck, J. Lin, and A. K. Pattanayak, Phys. Rev. E **95**, 062222 (2017).
[18] M. Kumari and S. Ghose, Phys. Rev. A **99**, 042311 (2019).
[19] J. Gong and P. Brumer, Phys. Rev. Lett. **90**, 050402 (2003).
[20] R. M. Angelo and K. Furuya, Phys. Rev. A **71**, 042321 (2005).
[21] M. Znidaric and T. Prosen, Phys. Rev. A **71**, 032103 (2005).
[22] Ph. Jacquod, Phys. Rev. Lett. **92**, 150403 (2004).
[23] Ph. Jacquod and C. Petitjean, Adv. Phys. **58**, 67 (2009).
[24] A. D. Ribeiro and R. M. Angelo, Phys. Rev. A **82**, 052335 (2010).
[25] A. D. Ribeiro and R. M. Angelo, Phys. Rev. A **85**, 052312 (2012).
[26] J. R. Klauder and B. S. Skagerstan, *Coherent States. Applications in Physics and Mathematical Physics* (World Scientific, Singapore, 1985).
[27] A. Perelomov, *Generalized Coherent States and their Applications* (Springer-Verlag, Berlim, 1986).
[28] W. M. Zhang, D. H. Feng, and R. Gilmore, Rev. Mod. Phys. **62**, 867 (1990).
[29] J. R. Klauder, Phys. Rev. D **19**, 2349 (1979).
[30] Y. Weissman, J. Phys. A **16**, 2693 (1983).
[31] E. A. Kochetov, J. Phys. A **31**, 4473 (1998).
[32] M. Baranger, M. A. M. de Aguiar, F. Keck, H. J. Korsch, and B. Schellaas, J. Phys. A **34**, 7227 (2001).
[33] A. D. Ribeiro, M. A. M. de Aguiar, and M. Baranger, Phys. Rev. E **69**, 066204 (2004).
[34] C. Braun and A. Garg, J. Math. Phys. **48**, 032104 (2007).
[35] H. Solari, J. Math. Phys. **28**, 1097 (1987).
[36] V. R. Vieira and P. D. Sacramento, Nucl. Phys. B **448**, 331 (1995).
[37] E. A. Kochetov, J. Math. Phys. **36**, 4667 (1995).
[38] M. Stone, K. S. Park, and A. Garg, J. Math. Phys. **41**, 8025 (2000).
[39] A. D. Ribeiro, M. A. M. de Aguiar, and A. F. R. de Toledo Piza, J. Phys. A **39**, 3085 (2006).
[40] A. L. Foggiatto and A. D. Ribeiro, Prog. Theor. Exp. Phys. **10**, 103A01 (2017).
[41] N. Bleistein and R. A. Handelsman, *Asymptotic Expansion of Integrals* (Dover, New York, 1986).
[42] A. Donoso and C. C. Martens, Phys. Rev. Lett. **87**, 223202 (2001).
[43] W. H. Miller, J. Chem. Phys. **136**, 210901 (2012).
[44] P. P. de M. Rios and A. M. Ozorio de Almeida, J. Phys. A: Math. Gen. **35**, 2609 (2002)
[45] T. Dittrich, C. Viviescas and L. Sandoval, Phys. Rev. Lett. **96**, 070403 (2006).
[46] T. Dittrich, E. A. Gómez and L. A. Pachón, J. Chem. Phys. **132**, 214102 (2010).
[47] A. L. Xavier Jr. and M. A. M. de Aguiar, Phys. Rev. Lett. **79**, 3323 (1997).
[48] M. Novaes, Phys. Rev. A **72**, 042102 (2005).
[49] M. A. M. de Aguiar, M. Baranger, L. Jaubert, F. Parisio and A. D. Ribeiro, J. Phys. A: Math. Gen. **38**, 4645 (2005).
[50] We recall that our complex phase-space can also be mapped onto an extended real phase-space, according to Refs. [47, 51].
[51] R. S. Kaushal and H. J. Korsch, Phys. Lett. A **276**, 47 (2000).
[52] L. S. Silveira and R. M. Angelo, Phys. Rev. A **95**, 062105 (2017).